Interface passivation using choline acetate for efficient and stable planar perovskite solar cells

M. Thambidurai[1, 2, 3], Herlina Arianita Dewi[2], Wang Xizu[3], Nripan Mathews[2,4], Cuong Dang[1,2], and Hung D. Nguyen*[1,2]*

1. School of Electrical and Electronic Engineering, Nanyang Technological University, 50 Nanyang Avenue, 639798, Singapore.
2. Energy Research Institute @NTU (ERI@N), Research Techno Plaza, X-Frontier Block, Level 5, 50 Nanyang Drive, 637553, Singapore.
3. Institute of Materials Research and Engineering (IMRE), Agency for Science, Technology and Research, 138634, Singapore.
4. School of Materials Science and Engineering, Nanyang Technological University, 50 Nanyang Avenue, 639798, Singapore.

*Email: hcdang@ntu.edu.sg; hunghtd@ntu.edu.sg

Abstract: In order to enhance the efficiency and robustness of perovskite solar cells (PSCs), surface passivation is crucial to minimize surface defects, improve charge transfer, and inhibit the penetration of deteriorating agents. In this study, we demonstrate that choline acetate (ChAc) can effectively passivate the surfaces of perovskites to improve their stability and photovoltaic performance. The perovskite film passivated with ChAc shows many improvements, such as greater crystallinity, smoother surface topography, preferable alignment of energy levels, and lower defect density. As a result, the champion power conversion efficiency (PCE) for the pristine and ChAc PSCs is 18.20% and 19.80%, respectively. The passivated PSCs also display superior stability, as evidenced by retained unencapsulated PCE of 93% after 600 hours of storage at ambient conditions and 40% relative humidity at 25 °C, compared to 85% retained for pristine PSCs. Our results provide a straightforward and very efficient way to produce high-performing and stable PSCs.

Keywords: Perovskite solar cells, moisture stability, surface defects passivation, interface,

1. Introduction

Recent developments in the field of photovoltaic applications have received considerable attention from researchers in organic-inorganic hybrid perovskite materials due to their favorable optical band gap, high absorption coefficient, low exciton binding energy, long carrier diffusion length, and higher carrier mobility.[1–7] Perovskite solar cells (PSCs) have achieved a rapid rise in PCE, rising from 3.8% in 2009 to 25.7% in 2023.[89] This unprecedented speed of advancement marks a significant milestone in the history of solar development. Furthermore, PSCs show a promising future for commercialization thanks to their easy fabrication process and low-cost materials. To be widely commercialized, several challenges must first be addressed, particularly with regard to long-term instability caused by ion migration and oxidation or humidity-related degradation. [10–15] The approach of passivation has been demonstrated to be a successful tactic for suppressing non-radiative recombination losses, reducing perovskite defects, and enhancing the performance and stability of PSCs.[16–19] Numerous modification techniques have consistently been suggested to minimize the surface defect of the perovskite active layer. For instance, the uncoordinated ions at the perovskite surface have been removed using certain halide salts (formamidinium chloride, 4-fluoro-phenethylammonium iodide, and tetra-ethyl ammonium iodide) as additives and/or modifiers.[20–24] In a variety of energy-related applications, ionic liquids (ILs), non-volatile salts with outstanding thermal stability, are now more often used. Device stability and performance have significantly increased with the addition of IL to PSCs.[25–27] By incorporating 1,3-dimethyl-3-imidazolium hexafluorophosphate (DMIMPF6) as the passivation layer between perovskites and Spiro-OMeTAD, Zhu and coworkers recorded an increased degree of hydrophobicity, long-term stability, and power conversion efficiency (PCE).[28] The defects on the surface and grain boundary of perovskite films were passivated using 4-chloro-1,8-naphthalic anhydride, which led to a

decrease in trap state density and an increase in carrier lifetime.[29] By adding 1-hexyl-3-methylimidazolium iodide (HMII) to PSCs, Akin and coworkers were able to enhance crystallinity and achieve a PCE of 20.6%.[30] Patil and coworkers utilized Guanidine acetate as an interface modifier between the hole transport layer (HTL) and the perovskite, leading to better energy level matching, lower defect densities, and less charge recombination.[31] Choline chloride (ChCl) was utilized to passivate the perovskite surface by Wang and coworkers, and it was discovered to be successful in extending carrier lifetime and improving moisture/thermal stability.[32] Hence, it is possible to anticipate that passivation materials will increase the PCE and stability of perovskite devices. For further advancements in PCE and stability of perovskites, it is essential to ascertain the effects of suitable morphology, surface defect, hydrophobicity, and optoelectronic properties.[33–35] A choline-based ionic liquid called choline acetate can be effectively used to dissolve microcrystalline cellulose. Moreover, it has been suggested that ILs could be recycled and reused due to their low melting point, non-volatility, and thermal stability. In addition, functional IL can promote hydrogen bonding, coordination, and electrostatic interactions between perovskites and ILs when needed, improving the crystallization tendency for high-quality films with fewer defects and increasing the water insensitivity with hydrophobic ILs. [36,37] Herein, using choline acetate (ChAc) as a surface passivating material, we demonstrate that the fabricated PSCs can exhibit improved stability and photovoltaic performance. For perovskite passivated with ChAc, the crystallinity, surface topography, energy levels alignment, and defect density are enhanced. Consequently, the unencapsulated pristine and ChAc passivated PSCs enable to yield champion PCE of 18.20% and 19.80%; with 85% and 93% retained PCEs as compared to their original value after 600 hours of storage at ambient condition can be achieved. This study highlights the importance of surface passivation to simultaneously enhance both stability and efficiency.

2. Experimental Section:

Materials: Fluorine-doped tin oxide (FTO) glass substrates were purchased from Nippon sheet glass Co., Ltd. (Japan). We purchased lead (II) iodide and lead (II) bromide from Tokyo Chemical Industry (TCI). Methylammonium bromide and formamidinium iodide were purchased from Dyesol. The following chemicals were purchased from Sigma Aldrich: Choline acetate (ChAc), Acetonitrile, Isopropyl alcohol, dimethylformamide, dimethyl sulfoxide, 2-methoxyethanol, titanium (IV) butoxide, acetylacetone, tin (II) chloride, and 4-tert-Butylpyridine. Spiro−OMeTAD was purchased from Luminescence technology corp.

Device Fabrication: The cleaning process involved ultrasonically cleaning the fluorine-doped tin oxide conducting glass (FTO) substrates for 20 min in mild detergent, deionized water, acetone, ethanol, and isopropanol, respectively. After that, nitrogen was used to dry the FTO substrates, and 20 minutes of ozone treatment followed. The compact-TiO_2 layer was deposited at the FTO glass substrate through a spin coating approach with a precursor solution containing titanium (IV) butoxide, acetylacetone, and 2-methoxyethanol and annealed at 500 °C for 1 h. After that, SnO_2 was spin-coated on the FTO/TiO_2 surface with a precursor solution containing tin (II) chloride and ethanol. The layer was annealed at 200 °C for 1 h. The following materials were used to make the perovskite solution: MABr (28 mg), FAI (215 mg), PbI_2 (0.633 mg), $PbBr_2$ (101 mg), 52.6 μL of the CsI (390 mg of CsI in 1mL of DMSO), and 1 mL of a mixed of DMF and DMSO solvents. Perovskite layers were fabricated using spin coating techniques at 1000 rpm for 10 s and 6000 rpm for 30 s, respectively. 100 μL of chlorobenzene was added to the rotating substrate during the final 15 seconds as an anti-solvent. Then, the as-deposited film was placed to a hot plate and annealed at 100 °C for 1h. The Choline acetate (ChAc) passivator was dissolved in 2-proponal to prepare precursor solutions of 0, 2, 4, and 6 mg/mL. The Spiro-OMeTAD solution was prepared by mixing

Spiro-OMeTAD powder (70 mg) with chlorobenzene (1 mL), 4-tertbutylpyridine (28 μL), lithium bis(trifluoromethanesulfonyl)imide solution (520 mg/mL in acetonitrile;17 μL) and cobalt (III) FK209 (376 mg in 1 mL of acetonitrile: 35 μL). The spiro-OMeTAD solution was spun coated onto the perovskite at 4000 rpm for 30 seconds. Finally, the gold (Au) back electrode was deposited by thermal evaporation.

Characterization: XRD measurements were carried out using an X-Ray diffractometer (Bruker D8 Advance). The surface morphology of the perovskite films was characterized using a FESEM (JEOL JSM−7600F). The XPS and UPS spectra of the perovskite samples were analyzed using a Kratos AXIS Supra. Contact angle measurements were taken using Dataphysics OCA−15 Pro. The absorption spectra of samples were measured using a UV-vis spectrophotometer (UV−1800, Shimadzu). Photoluminescence (PL) spectra were recorded using an RF−5301PC (Shimadzu) spectrophotometer. The current density-voltage (J-V) curve of the device was measured using a Keithley 2612A source meter with an AM 1.5G illumination (100 $mWcm^{-2}$). The IPCE spectra were recorded with a PVE300 (Bentham).

3. Results and Discussion

Figure 1a displays a schematic of a planar n-i-p PSC configuration comprising fluorine-doped tin oxide (FTO) as the anode, a compact TiO_2/SnO_2 layer as the electron transport layer (ETL), a perovskite layer as the light-absorbing layer, Spiro-MeOTAD as the hole transport layer (HTL), and gold as the cathode. The J-V characteristics of PSCs with various ChAc concentrations were measured under AM1.5 G illumination, and the corresponding photovoltaic characteristics, including their open-circuit voltage (V_{oc}), short-circuit current (J_{sc}), fill factor (FF), and power conversion efficiency (PCE), are presented in **Figure 1b** and **Table S1**. To achieve the optimum content, the ChAc concentrations in the isopropyl alcohol precursor solution were varied from 0

to 6 mg/mL. When the ChAc concentration is raised from 2 to 4 mg/mL, the PCE increases, and the PSCs with the 4 mg/mL ChAc passivated exhibit the best device performance. The pristine PSCs displayed a PCE of 18.20%, V_{oc} of 1.09V, J_{sc} of 22.30 mA cm^{-2}, and FF factor of 74.69%. On the other hand, the 4 mg/mL ChAc passivated device showed a V_{oc} of 1.12 V, J_{sc} of 22.70 mA cm^{-2}, and FF of 77.63%, leading to a significantly greater PCE of 19.80%. The performance of the device is reduced as the ChAc concentration is raised further to 6% (**Figure S1** and **Table S1**). A statistical distribution of photovoltaic parameters (V_o, J_{sc}, FF, and PCE) of PSCs with and without the addition of ChAc is shown in **Figure 1c** and **Figure S2** to demonstrate the repeatability of the device. The average PCEs of pristine and ChAc passivated devices are 17.52%, and 19.30%, respectively. The repeatability of the PSCs device is undoubtedly improved by the addition of ChAc. According to incident photon-to-current efficiency (IPCE) results, the integrated J_{sc} values for the pristine and ChAc passivated devices were 19.98 and 20.65 mA cm^{-2}, respectively; this result was comparable to the J-V measurement values, as displayed in **Figure 1c**.

X-ray diffraction (XRD) measurements were carried out to explore the impact of the ChAc on the crystallinity of perovskite films, as presented in **Figure 2a**. Both the pristine and passivated perovskite films exhibited identical crystal structures. There were no additional peaks in the passivated films, indicating that films passivated with ChAC could reduce perovskite defects without altering crystal structure. The ChAc interfacial modifier contributes to enhancing the crystallization of the perovskite film since it increases peak intensities and decreases FWHM values (0.33 to 0.25) relative to the pristine film. Field emission scanning electron microscopy (FESEM) measurements of the perovskite films were performed to observe the ChAc-induced changes in the microstructure on the perovskite layer, as displayed in **Figure 2b-c & Figure S3** . The FESEM images show that both the pristine and ChAc passivated surfaces exhibit

homogeneous, compact, smooth surface morphology, with the grain size of the passivated surface being slightly larger than that of the pristine surface (**Figure S4**) .

We performed x-ray photoelectron spectroscopy (XPS) on both the pristine and passivated with ChAc to investigate the interaction between the ChAc and the perovskite film. The XPS analysis (**Figure 2d)** shows that the pristine Pb 4f XPS has two peaks at about 143.3 eV and 138.4 eV, which are attributable to Pb $4f_{5/2}$ and Pb $4f_{7/2}$, respectively. Since the pronounced peaks of Pb $4f_{5/2}$ and Pb $4f_{7/2}$ were shifted to lower binding energies of 143.0 and 138.1 eV, respectively, in the passivated ChAc, it appears that Pb^{2+} has been effectively passivated. In the pristine film, there are two peaks assigned to metallic Pb^0 at 136.7 and 141.6 eV, while no metallic Pb^0 peak is observed in the passivated film, suggesting that the ChAc suppresses the non-radiative recombination.[38,39]

In order to determine the effect of ChAc on the optical properties of perovskite films, the ultraviolet-visible (UV-vis) absorption and photoluminescence (PL) spectra were analyzed. The absorption spectra of pristine and passivated films are illustrated in **Figure S5**. From the comparison of the absorption intensities, it can be seen that the ChAc-modified perovskite films have a slightly higher absorption intensity. We studied the surface morphology of pristine and passivated ChAc perovskites using an atomic force microscope. The roughness of the passivated film (17.6 nm) is smaller than that of the perovskite film (24.4 nm), as shown in **Figure 3a-b**, showing the effect of ChAc to smoothen the surface. The PL spectra of perovskite films with and without ChAc are displayed in **Figure 3c**. A comparison of the steady-state PL spectra of pristine and ChAc passivated films showed no significant differences in peak positions, indicating that the ChAc did not affect the optical bandgap of the perovskites. The PL intensity was significantly increased for the ChAc passivated film, indicating fewer defects in the ChAc passivated perovskite films, and consequently minimized non-radiative recombination.[40,41]

To verify the passivation effect of ChAc on the perovskite, we conducted the space-charge limited current (SCLC) measurement of pristine and ChAc passivated devices. **Figure 3d** illustrates dark I-V curves of the devices with a configuration of FTO/TiO_2/SnO_2/perovskite (with and without ChAc)/PCBM/Ag. For the electron-only devices using both pristine and ChAc passivated layers, the V_{TFL} values were measured to be 0.35, and 0.25 V, respectively. The equation $N_{trap} = 2\varepsilon\varepsilon_0 V_{TFL}/eL^2$ was used to obtain the trap density (N_{trap}) of the films, where L, ε, ε_0 and e represents the film thickness of perovskite, the relative dielectric constant of perovskite, vacuum permittivity, and elemental charge, respectively.[42,43] The N_{trap} values for pristine and ChAc passivated films were calculated to be 2.69 x 10^{15} cm^{-3} and 1.92 x 10^{15} cm^{-3}, respectively. The presence of ChAC greatly reduced the trap density of perovskites.

To examine the electrical characteristics and energy levels, ultraviolet photoelectron spectroscopy (UPS) measurements were performed. Based on the results of UPS (**Figure 4a-b, & d-e**) and the band gap (E_g), the work function (WF), valence band maximum (VBM), and conduction band minimum (CBM) of the perovskite films are determined. According to **Figure 4c**, the E_g values of pristine and ChAc passivated films are determined using the Tauc plot to be 1.63 and 1.62 eV, respectively. It is observed that the pristine perovskite films exhibit WF, VBM, and CBM values of -4.21, -5.71, and -4.08 eV, respectively. The ChAc passivated films included associated WF, VBM, and CBM values of -4.09, -5.63, and -4.01 eV, respectively. In contrast to pristine film, the ChAc passivated film's VBM and CBM display better energy level alignment, as seen in **Figure 4f**, which reduces the interfacial energy barrier and reduces non-radiative recombination.

The hydrophobicity of perovskite films is studied by measuring the water contact angles, which are displayed in **Figure S6**. With respect to the water contact angle, pristine and ChAc passivated perovskite films showed values of 44° and 51°, respectively, revealing the superior moisture

stability for the ChAc passivated film. The effect of ChAc surface passivation to enhance the perovskite film stability was assessed using XRD and UV-vis spectra, while the respective PSCs were characterized by measuring the trend of PCE as a function of time. Both films and PSCs were stored under the same storage conditions (in the dark and at 40% RH). While the unavoidable perovskite degradation into PbI_2 was still observed, the ChAc passivation indeed showed its enhanced moisture resistance behavior. After 600 hours of aging, the absorbance of the pristine decreased by 13%, but only by 7% for the film with ChAc (**Figure 5a**), suggesting less PbI_2 formation upon passivation. This is also supported by the results of **Figure 5b**, which show that the ratio of integrated XRD area at PbI_2 peak to that at the perovskite peak was only 0.6:1 for ChAc passivated films in contrast to 1.4:1 for the pristine films. Shelf stability measurements were conducted with PSCs kept in the dark and at 40% RH as shown in **Figure 5c-f**. No encapsulation was used in the testing of all devices. After 600 hours of shelf storage, the ChAc passivated device keeps over 93% of its initial PCE, whereas the pristine device only retains 85%. This result clearly shows that adding ChAc enhances the PSCs' moisture stability, in agreement with the contact angle and film characterizations.

4. Conclusions

In summary, choline acetate (ChAc) is utilized to passivate perovskite surface defects and to improve both PCE and stability of the PSCs. With ChAc passivated perovskites, the crystallinity and surface topography are improved, with better energy levels alignment and minimized defect density. As a result, PSCs with ChAc had an enhanced power conversion efficiency (PCE) of 19.80% in contrast to pristine devices of 18.20%. In addition, unencapsulated devices with ChAC maintained 93% of their initial efficiency after aging for 600 hours at a relative humidity of 40%, revealing superior stability compared to 85% of the pristine devices. With the proposed passivation

technique, which improves the performance and stability of the PSC by defect passivation, perovskites-based optoelectronic devices will get a wider range of practical applications.

Acknowledgments: The research is supported by the AcRF Tier2 grant (MOE-T2EP50121-0012) and AcRF Tier1 grant RG60/22 from the Singapore Ministry of Education, and the EMA-EP004-EKJGC-0003 grant from the Energy Market Authority (EMA) Singapore. The Merlion program given by the French Ministry of Europe and Foreign Affairs (MEAE), and the Singaporean Partner, Nanyang Technological University, Singapore. We would like to thank Prof. Madhavi Srinivasan at Energy Research Institute @ NTU (ERI@N) for supporting this work.

References

1 L. Yang, J. Feng, Z. Liu, Y. Duan, S. Zhan, S. Yang, K. He, Y. Li, Y. Zhou, N. Yuan, J. Ding and S. Liu, *Adv. Mater.*, 2022, **34**, 2201681.

2 M. Li, H. Li, Q. Zhuang, D. He, B. Liu, C. Chen, B. Zhang, T. Pauporté, Z. Zang and J. Chen, *Angew. Chemie*, 2022, 134, e202206914.

3 Y. Zhang, L. Xu, Y. Wu, Q. Zhou, Z. Shi, X. Zhuang, B. Liu, B. Dong, X. Bai, W. Xu, D. Zhou and H. Song, *Nano Energy*, 2021, **90**, 106610.

4 S. Zhan, Y. Duan, Z. Liu, L. Yang, K. He, Y. Che, W. Zhao, Y. Han, S. Yang, G. Zhao, N. Yuan, J. Ding and S. Liu, *Adv. Energy Mater.*, 2022, **12**, 2200867.

5 H. Min, D. Y. Lee, J. Kim, G. Kim, K. S. Lee, J. Kim, M. J. Paik, Y. K. Kim, K. S. Kim, M. G. Kim, T. J. Shin and S. Il Seok, *Nature*, 2021, **598**, 444–450.

6 M. Thambidurai, F. Shini, P. C. Harikesh, N. Mathews and C. Dang, *J. Power Sources*, 2020, **448**, 227362.

7 C. Liu, S. Liu, Y. Wang, Y. Chu, K. Yang, X. Wang, C. Gao, Q. Wang, J. Du, S. Li, Y. Hu, Y. Rong, L. Guo, A. Mei and H. Han, *Adv. Funct. Mater.*, 2021, **31**, 2010603.

8 A. Kojima, K. Teshima, Y. Shirai and T. Miyasaka, *J. Am. Chem. Soc.*, 2009, **131**, 6050–6051.

9 Best Research-Cell Efficiency Chart, https://www.nrel.gov/pv/assets/pdfs/best-research-cell-efficiencies.20200218.pdf, (accessed 6 March 2020).

10 G. Tumen-Ulzii, T. Matsushima, D. Klotz, M. R. Leyden, P. Wang, C. Qin, J. W. Lee, S. J. Lee, Y. Yang and C. Adachi, *Commun. Mater.*, 2020, **31**, 1–7.

11 S. Mazumdar, Y. Zhao and X. Zhang, *Front. Electron.*, 2021, **2**, 1–34.

12 L. Duan and A. Uddin, *Mater. Chem. Front.*, 2022, **6**, 400–417.

13 Y. Zhou, Y. Yin, X. Zuo, L. Wang, T. De Li, Y. Xue, A. Subramanian, Y. Fang, Y. Guo, Z. Yang, M. Cotlet, C. Y. Nam and M. H. Rafailovich, *Chem. Mater.*, 2021, **33**, 6120–6135.

14 L. Duan, D. Walter, N. Chang, J. Bullock, D. Kang, S. P. Phang, K. Weber, T. White, D. Macdonald, K. Catchpole and H. Shen, *Nat. Rev. Mater.*, 2023, 8, 261-281.

15 Y. Cheng and L. Ding, *Energy Environ. Sci.*, 2021, **14**, 3233–3255.

16 W. Shen, Y. Dong, F. Huang, Y.-B. Cheng and J. Zhong, *Mater. Reports Energy*, 2021, 1, 100060.

17 Y. Zou, R. Guo, A. Buyruk, W. Chen, T. Xiao, S. Yin, X. Jiang, L. P. Kreuzer, C. Mu, T. Ameri, M. Schwartzkopf, S. V. Roth and P. Müller-Buschbaum, *ACS Appl. Mater. Interfaces*, 2020, **12**, 52643–52651.

18 Y. Shi, E. Rojas-Gatjens, J. Wang, J. Pothoof, R. Giridharagopal, K. Ho, F. Jiang, M. Taddei, Z. Yang, E. M. Sanehira, M. D. Irwin, C. Silva-Acuña and D. S. Ginger, *ACS Energy Lett.*, 2022, **7**, 4081–4088.

19 N. Mozaffari, T. Duong, M. M. Shehata, A. D. Bui, H. T. Pham, Y. Yin, Y. O. Mayon, J. Zheng, M. A. Mahmud, G. D. Tabi, G. G. Andersson, L. E. Black, J. Peng, H. Shen, T. P. White, K. Weber and K. R. Catchpole, *Sol. RRL*, 2022, 6, 2200355.

20 X. Jiang, S. Chen, Y. Li, L. Zhang, N. Shen, G. Zhang, J. Du, N. Fu and B. Xu, *ACS Appl. Mater. Interfaces*, 2021, **13**, 2558–2565.

21 A. Ciccioli, R. Panetta, A. Luongo, B. Brunetti, S. Vecchio Ciprioti, M. L. Mele and A.

Latini, *Phys. Chem. Chem. Phys.*, 2019, **21**, 24768–24777.

22 S. You, X. Xi, X. Zhang, H. Wang, P. Gao, X. Ma, S. Bi, J. Zhang, H. Zhou and Z. Wei, *J. Mater. Chem. A*, 2020, **8**, 17756–17764.

23 F. Shini, M. Thambidurai, H. A. Dewi, N. F. Jamaludin, A. Bruno, A. Kanwat, N. Mathews, C. Dang and H. D. Nguyen, *J. Mater. Chem. C*, 2022, **10**, 9044–9051.

24 Y. Yu, J. Xia and Y. Liang, *AIP Adv.*, 2022, 12, 055307.

25 F. Wang, D. Duan, M. Singh, C. M. Sutter-Fella, H. Lin, L. Li, P. Naumov and H. Hu, *Energy Environ. Mater.*, 2022, 1–21.

26 T. Wang, W. Deng, J. Cao and F. Yan, *Adv. Energy Mater.*, 2022, **2201436**, 1–35.

27 M. Shahiduzzaman, E. Y. Muslih, A. K. M. Hasan, L. Le Wang, S. Fukaya, M. Nakano, M. Karakawa, K. Takahashi, M. Akhtaruzzaman, J. M. Nunzi and T. Taima, *Chem. Eng. J.*, 2021, **411**, 128461.

28 X. Zhu, M. Du, J. Feng, H. Wang, Z. Xu, L. Wang, S. Zuo, C. Wang, Z. Wang, C. Zhang, X. Ren, S. Priya, D. Yang and S. Liu, *Angew. Chemie - Int. Ed.*, 2021, **60**, 4238–4244.

29 B. Shi, Y. Li, F. Gao, J. Li, X. Cai, C. Zhang, Y. Wu, C. Lu, J. Wang and S. Liu, *Adv. Mater. Interfaces*, 2022, 2201809.

30 S. Akin, E. Akman and S. Sonmezoglu, *Adv. Funct. Mater.*, 2020, 30, 2002964.

31 P. Patil, D. S. Mann, S. R. Rondiya, N. Y. Dzade, S. N. Kwon and S. I. Na, *Sol. RRL*, 2021, **5**, 2100547 (1–10).

32 Z. Wang, R. Li, M. Zhang and M. Guo, *Ceram. Int.*, 2022, **48**, 212–223.

33 C. Zhi, S. Wang, S. Sun, C. Li, Z. Li, Z. Wan, H. Wang, Z. Li and Z. Liu, *ACS Energy lett*. 2023, 8, 1424-1433.

34 X. Ji, K. Feng, S. Ma, J. Wang, Q. Liao, Z. Wang, B. Li, J. Huang, H. Sun, K. Wang and X. Guo, *ACS Nano*, 2022, **16**, 11902–11911.

35 B. Yang, J. Suo, F. Di Giacomo, S. Olthof, D. Bogachuk, Y. Kim, X. Sun, L. Wagner, F. Fu, S. M. Zakeeruddin, A. Hinsch, M. Gratzel, A. Di Carlo and A. Hagfeldt, *ACS Energy Lett.*, 2021, **6**, 3916–3923.

36 X. Zheng, W. Yu and S. Priya, *J. Energy Chem.*, 2018, **27**, 748–752.

37 M. Thambidurai, H. A. Dewi, A. Kanwat, S. S. Periyal, N. F. Jamaludin, A. Bruno, N. Mathews, C. Dang and H. D. Nguyen, *J. Power Sources*, 2023, **564**, 232874.

38 H. Choi, X. Liu, H. Il Kim, D. Kim, T. Park and S. Song, *Adv. Energy Mater.*, 2021, **11**, 2102189.

39 M. Thambidurai, M. I. Omer, F. Shini, H. A. Dewi, N. F. Jamaludin, T. M. Koh, X. Tang, N. Mathews and C. Dang, *ChemSusChem*, 2022, 15, 2102189.

40 D. Koo, Y. Cho, U. Kim, G. Jeong, J. Lee, J. Seo, C. Yang and H. Park, *Adv. Energy Mater.*, 2020, **10**, 2001920 (1–9).

41 Y. Xie, J. Duan, L. Peng, Arramel and N. Li, *Adv. Photonics Res.*, 2021, **2**, 2100012.

42 Y. Yang, J. Liang, Z. Zhang, C. Tian, X. Wu, Y. Zheng, Y. Huang, J. Wang, Z. Zhou, M. He, Z. Chen and C. C. Chen, *ChemSusChem*, 2022, 15, 2102474.

43 N. R. Jiang, Y. F. Wang, Q. F. Dong, C. Da Ge, Z. Q. Yang, D. Yin, Y. F. Liu, Y. G. Bi, J. Feng and H. B. Sun, *Sol. RRL*, 2021, **5**, 2000821 (1–8).

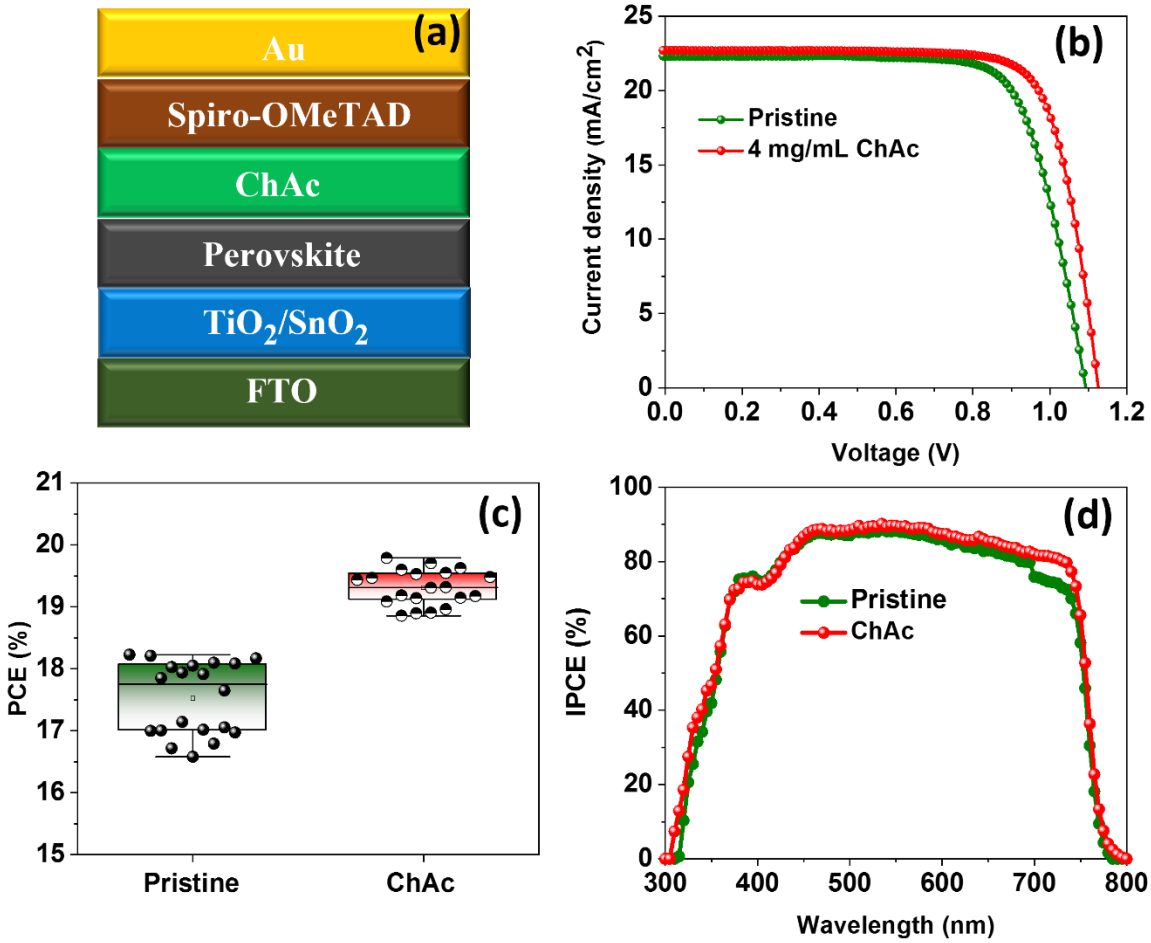

Figure 1. (a) Device structure, (b) J-V curves, (c) statistical distribution of PCE and (d) IPCE spectra of pristine and ChAc passivated planar PSCs.

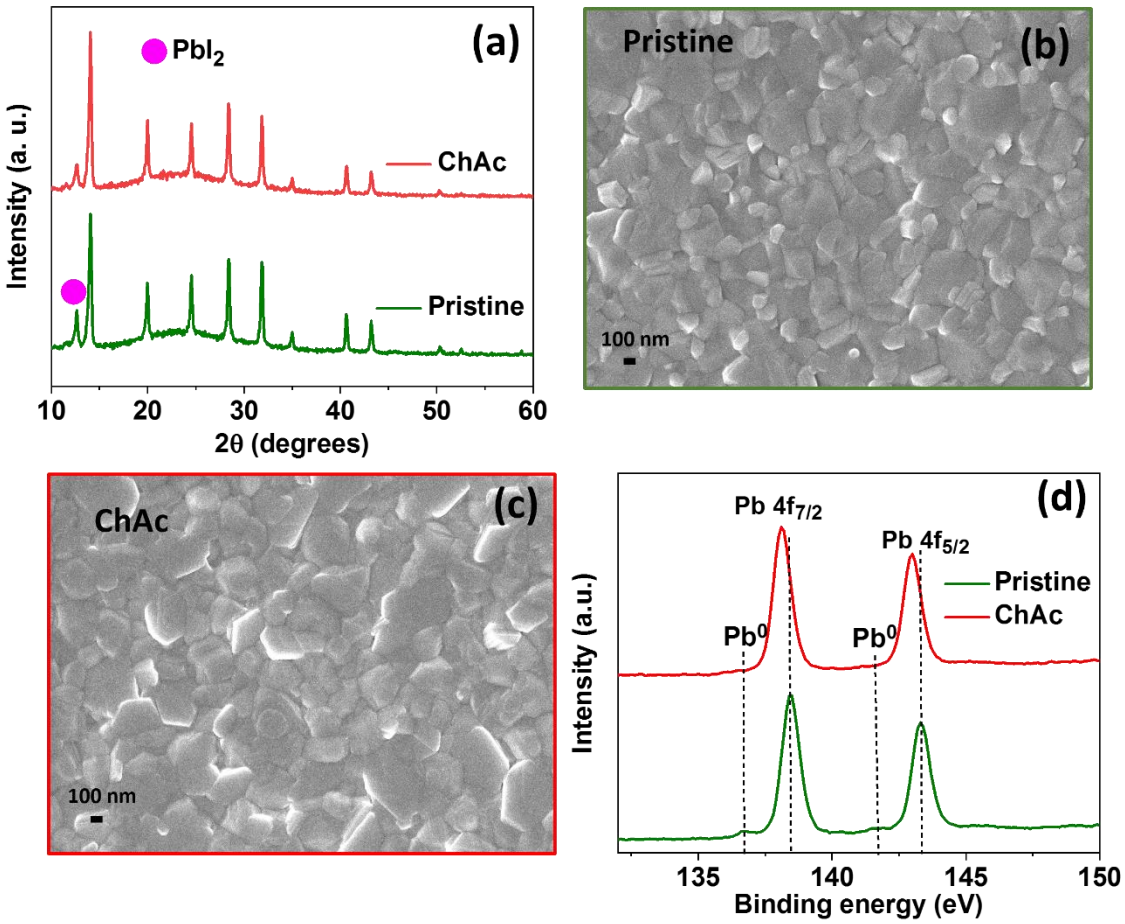

Figure 2. (a) X-ray diffraction patterns, (b-c) FESEM and (d) XPS spectra of the pristine and ChAc passivated PSCs.

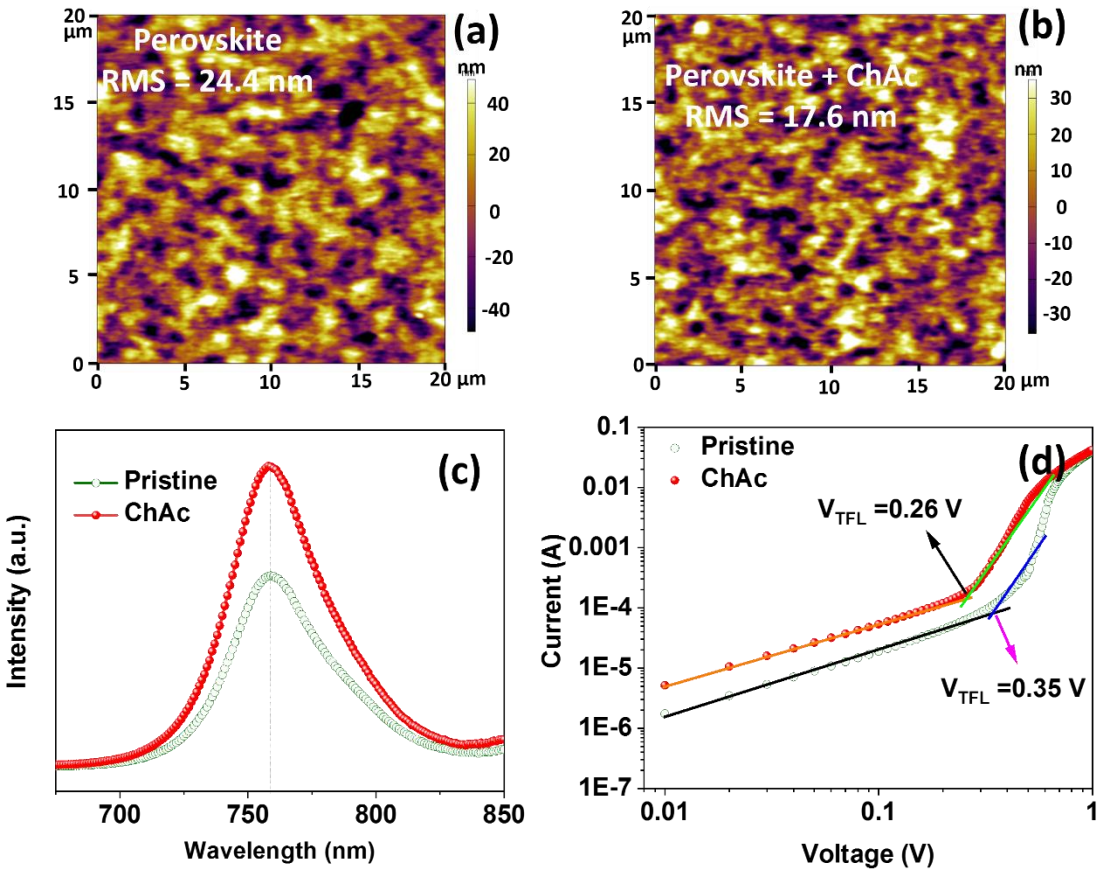

Figure 3. (a-b) AFM, (c) PL spectra and (d) SCLC of the pristine and ChAc passivated perovskite films.

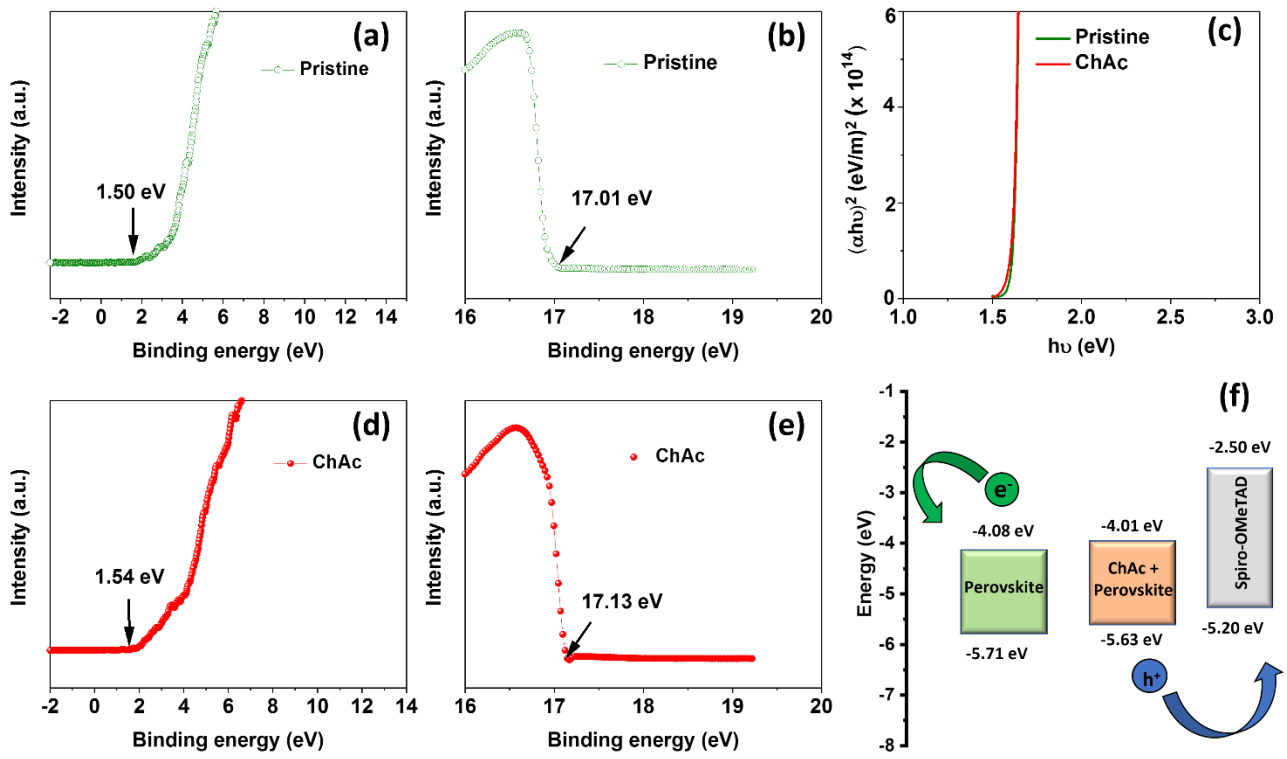

Figure 4. (a-b) UPS spectra of pristine perovskite film. (b) Tauc plot of the pristine and ChAs passivate perovskite films. (d-e) UPS spectra of ChAc passivated perovskite film. (f) Energy level alignment of perovskite device.

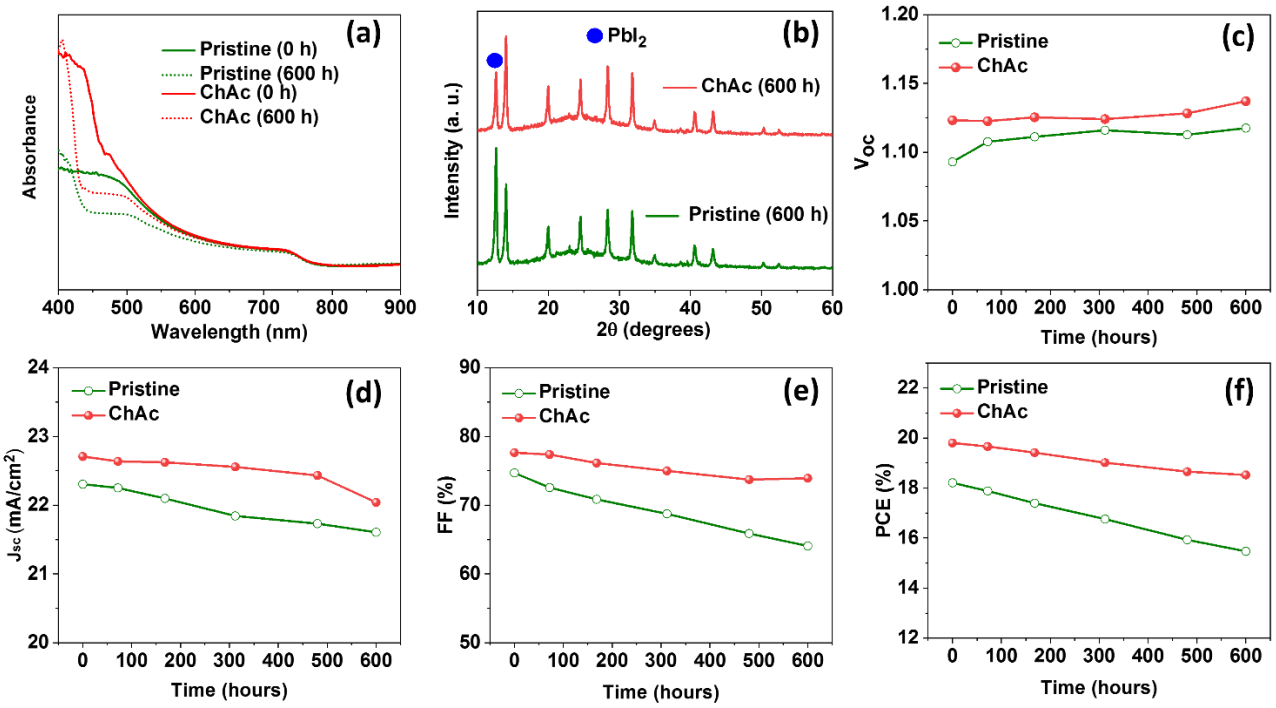

Figure 5. (a) Absorption spectra of pristine and ChAc passivated films before (0 h) and after aging (600 h). (b) XRD patterns of pristine and ChAc passivated perovskite films after aging (600 h). (c-f) An analysis of the V_{oc}, J_{sc}, FF and PCE decay rate of unencapsulated PSCs during ambient air storage with 40% relative humidity at room temperature.

Supporting information

Interface passivation using choline acetate for efficient and stable planar perovskite solar cells

M. Thambidurai[1, 2, 3], Herlina Arianita Dewi[2], Wang Xizu[3], Nripan Mathews[2,4], Cuong Dang[1,2], and Hung D. Nguyen*[1,2]*

1. School of Electrical and Electronic Engineering, Nanyang Technological University, 50 Nanyang Avenue, 639798, Singapore.
2. Energy Research Institute @NTU (ERI@N), Research Techno Plaza, X-Frontier Block, Level 5, 50 Nanyang Drive, 637553, Singapore.
3. Institute of Materials Research and Engineering (IMRE), Agency for Science, Technology and Research, 138634, Singapore.
4. School of Materials Science and Engineering, Nanyang Technological University, 50 Nanyang Avenue, 639798, Singapore.

*Email: hcdang@ntu.edu.sg; hunghtd@ntu.edu.sg

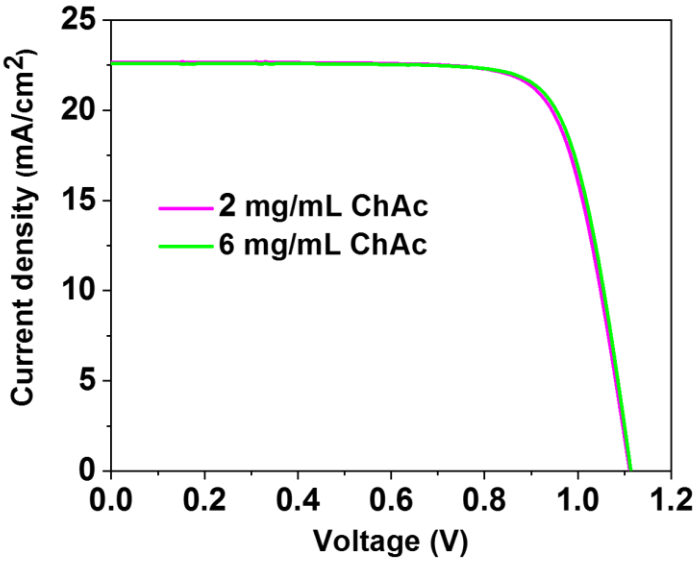

Figure S1. J-V curves of the ChAc passivated planar PSCs.

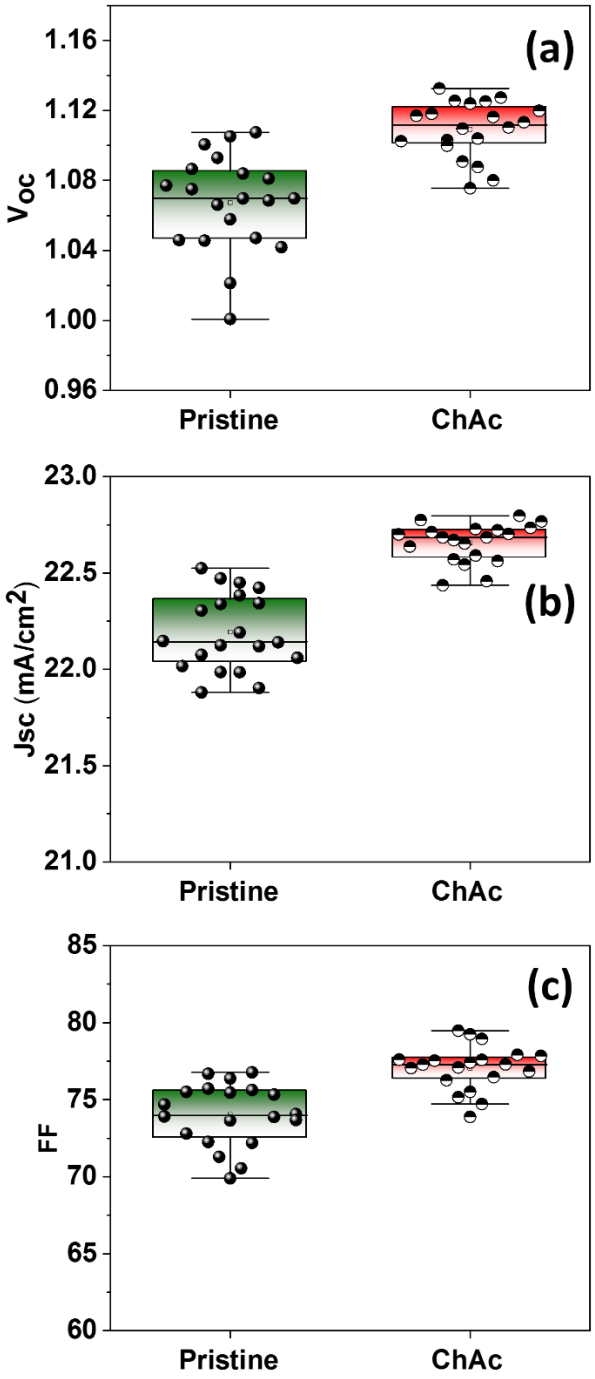

Figure S2. Statistical distribution of (a) V_{oc}, (b) J_{sc} and (c) FF of pristine and ChAc passivated planar PSCs.

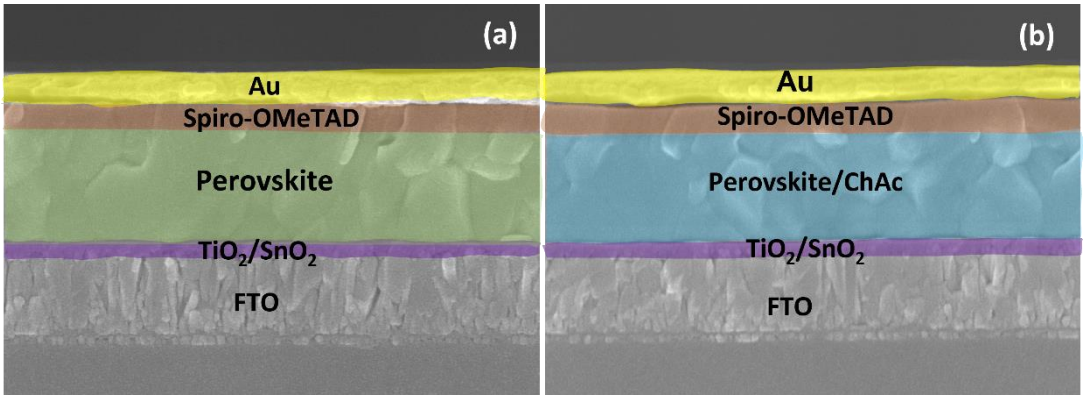

Figure S3. Cross-sectional FESEM images of (a) pristine and (b) 4 mg/mL ChAc PSCs.

The cross-sectional images of the perovskite solar cell without and with ChAc passivation are shown in Figure S3. The relative thickness of the perovskite layer for pristine and 4 mg/mL ChAc passivated perovskite layer was found to be similar at approximately 600 nm. Despite the additional ChAc layer added to the pristine device, the change in film thickness is unobservable using the FESEM images. This can be explained by the low ChAc concentration applied, making it difficult to distinguish the few nano-meters thin ChAc layer.

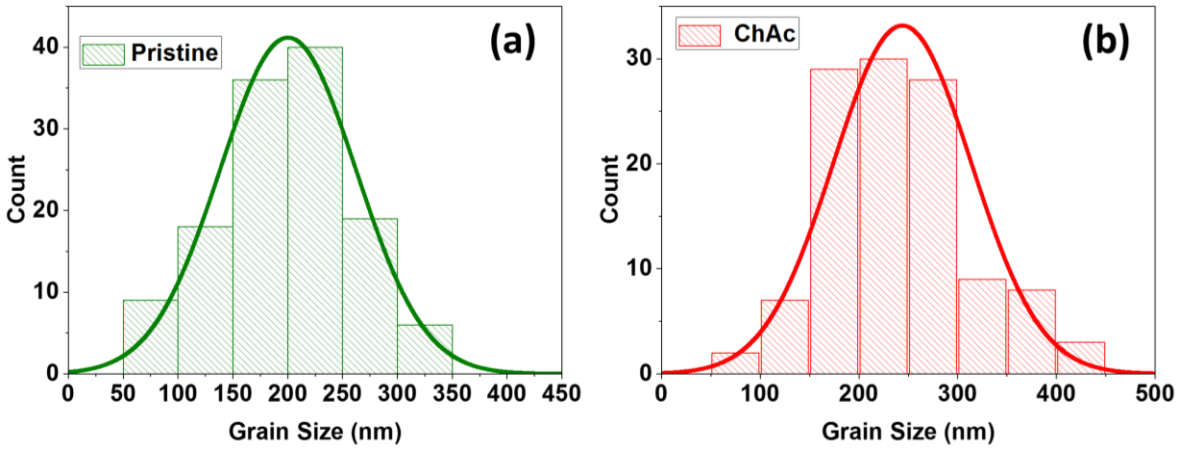

Figure S4. Grain size distribution of (a) pristine and ChAc passivated films.

The grain size distribution of pristine perovskite films with and without ChAc is illustrated in Figure S1. The average grain size of the pristine is estimated to be around 200 nm, however the passivated film with ChAc is found to be 245 nm.

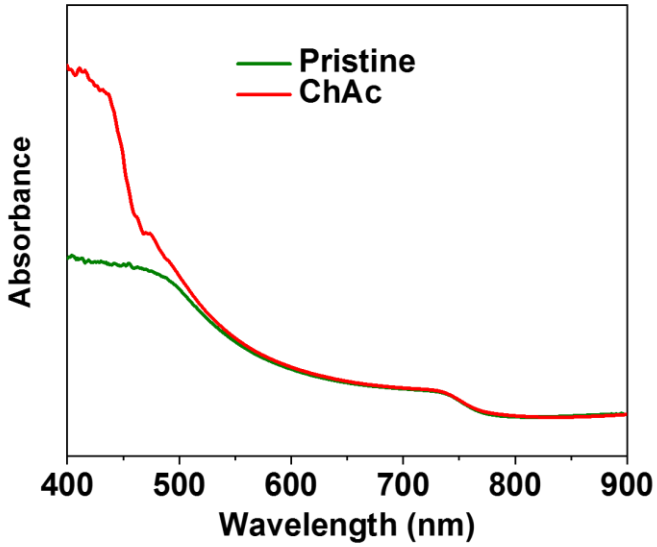

Figure S5. UV absorption spectra of pristine and ChAc passivated perovskite films.

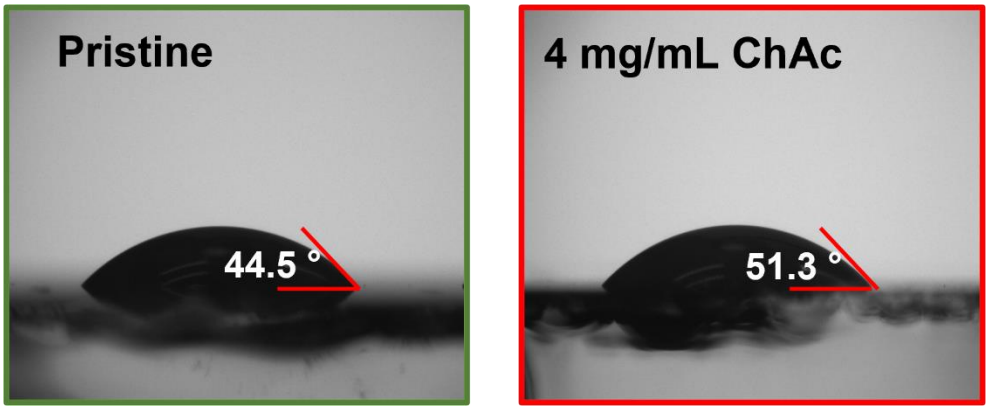

Figure S6. Water contact angles of the pristine and ChAc passivated perovskite films.

Table 1. Photovoltaic parameters of perovskite solar cells with and without ChAc passivation.

Devices	V_{oc} [V]	J_{sc} [mA cm^{-2}]	FF [%]	PCE [%]
Pristine	1.09	22.30	74.69	18.20
2 mg/mL ChAc	1.11	22.66	76.51	19.24
4 mg/mL ChAc	1.12	22.70	77.63	19.80
6 mg/mL ChAc	1.11	22.60	77.41	19.45